ResearchGate

See discussions, stats, and author profiles for this publication at: https://www.researchgate.net/publication/234893728

Study on Liquid–Vapor Interface of Water. I. Simulational Results of Thermodynamic Properties and Orientational Structure

ARTICLE *in* THE JOURNAL OF CHEMICAL PHYSICS · FEBRUARY 1988

Impact Factor: 2.95 · DOI: 10.1063/1.453919

CITATIONS
213

READS
16

2 AUTHORS:

Mitsuhiro Matsumoto
Kyoto University
62 PUBLICATIONS **1,581** CITATIONS
SEE PROFILE

Yosuke Kataoka
Hosei University
87 PUBLICATIONS **1,098** CITATIONS
SEE PROFILE

Available from: Yosuke Kataoka
Retrieved on: 26 January 2016

Study on liquid–vapor interface of water. I. Simulational results of thermodynamic properties and orientational structure

Mitsuhiro Matsumoto and Yosuke Kataoka
Department of Chemistry, Faculty of Science, Kyoto University, Kitashirakawa, Kyoto 606, Japan

(Received 14 September 1987; accepted 11 November 1987)

Molecular dynamics simulations have been carried out for liquid–vapor interface of water and also of Lennard-Jones system. Surface tension and surface excess energy are calculated, from which surface excess entropy is evaluated. These thermodynamic quantities suggest the existence of some liquid-structural change near the surface of water, which is not seen in Lennard-Jones system. For water, orientational structuring near the surface is studied and two types of orientation are found. In the vapor side, a water molecule has a tendency of projecting one hydrogen atom toward the vapor, and in the liquid side, a molecule prefers to lie down on the surface with both hydrogen atoms slightly directed to the liquid. From these results, surface potential χ can be evaluated to be about $+0.16$ V at $T = 300$ K, which confirms recent experimental results. The ellipticity coefficient is also discussed and the assumption often used in analysis of experimental results of ellipsometry is found to be inadequate for water due to the structural change. These observed orientational orderings are qualitatively consistent with results of molecular theory of surface recently developed and also with simulational results of water near hydrophobic walls.

I. INTRODUCTION

Concerning physical and chemical properties of liquid–vapor interface, water is of a peculiar character.[1–3] For example, the surface tension, which is equal to the surface excess Helmholtz free energy, is especially large and its temperature dependence, which corresponds to the surface excess entropy, is quite different from that of "simple" liquids. These are often attributed to some orientational ordering of molecules near the interface due to the hydrogen bonding, but the nature of the ordering is not so much understood yet even qualitatively. There is no need to mention, however, the importance of study on interface (of liquid–vapor, liquid–liquid, or liquid–solid) of aqueous systems, also from the viewpoint of applied chemistry and biological chemistry.[4,5]

Recently studies of interfacial systems of simple fluids such as a Lennard-Jones(LJ) system or a Stockmayer(LJ + point dipole) system have been fully developed. However, aqueous systems are much more difficult to treat theoretically or experimentally since the interaction between water molecules is very complicated. Computer simulation, with molecular dynamic (MD) or Monte Carlo (MC) methods, is therefore a useful technique to investigate what occurs near the interface. As far as we noticed, a MC calculation of Borštnik, Janežič, and Ažman[6] in 1980 is the first to simulate the liquid–vapor interfacial properties of water with MCY potential[7]; in that they reported the shape of the density profile, the surface tension, the excess energy, and the orientational structure of molecules, but the number of molecules they used, 64, appears to be too small to extract definite conclusion. Lee and Scott[8] used a MC umbrella sampling technique with 256 particles to calculate the surface tension of water and reported a value 97 ± 6 dyn/cm at 298 K for ST2 potential.[9] Townsend, Gryko, and Rice[10] also studied ST2 water (a free cluster of 1000 or 512 particles) at 300 K by MD simulation and confirmed the existence of orientational ordering (tendency to "lie in the surface").

Theoretical studies have much longer history. In 1951 Weyl[11] suggested by considering the difference of polarizability of the H and O atoms that water molecules near the surface have their dipoles directed toward the interior of liquid phase, i.e., O^{2-} is in the vapor side and H^+ is in the liquid side. Stillinger and Ben-Naim (SB)[12] obtained a similar result from electrostatic calculation of a simple model of water molecules (point dipole + point quadrupole). On the other hand, assuming a simple exponential decay of coherence and evaluating the surface excess free energy, Fletcher[13] concluded that the orientation of the lowest (free) energy is that with the protons directed *outwards*. Recently Croxton[14] adopted a model almost similar to that of SB and, by introducing a dipole order parameter, got the same result as Fletcher's. It appears, however, that the most relevant difference between the calculation of SB and that of Croxton is not the method itself, but the value of the quadrupole moment of the water molecule; SB used $Q_{zz} = +0.364$ D Å ($1\ \text{D Å} = 3.336 \times 10^{-40}\ \text{C m}^2$) and Croxton adopted the values of opposite sign ($Q_{xx} = -6.56$, $Q_{yy} = -5.18$, $Q_{zz} = -5.51$ D Å). The values of the quadrupole moment of water experimentally measured or quantum mechanically calculated most recently[15] are rather different from both of these; e.g., $Q_{xx} = +2.63$, $Q_{yy} = -2.50$, $Q_{zz} = -0.13$ D Å.[16] Considering that the orientational ordering is determined mostly by the coupling term of the dipole and the quadrupole,[14] it is natural that the change of the sign of the quadrupole moment causes the opposite predictions for orientation.

Now let us briefly review experimental results about the liquid–vapor interface of water. Of all thermodynamic quantities, the surface tension is probably the most direct and easily available one. Various empirical rules, including

 0021-9606/88/053233-13$02.10 © 1988 American Institute of Physics

Eötvös–Ramsay–Shields–Katayama's formula and the parachor of Sugden are found in many textbooks.[17–20] Water is "abnormal" also from that point of view; e.g., Good[1] calculated the surface entropy of various liquids and found that the value is extraordinarily low for water and other strongly hydrogen-bonded compounds in comparison with nonpolar or polar, but non-hydrogen-bonded ones. The existence of the thermal transitions around the room temperature which Drost-Hansen suggested[4] from the measurement of the surface tension of water is not accepted,[5,21,22] and an empirical smooth function is presented in analytic form.[23] The surface roughness of water is recently measured with x-ray reflection technique,[24] which can be compared with the results of ellipsometry[3,25]; the thickness of the transition zone is suggested to be much smaller than that of simple liquids.[3] The orientational ordering near the surface is, however, very difficult to estimate experimentally and the only information is obtained from the surface potential measurement. Since the measured electric potential difference includes the chemical potential difference, which is not easily estimated, the obtained potential values scatter very much, but their signs appear to be positive,[26] which suggests the dipole is more or less directed toward the liquid side. The ellipsometry technique can be also applied to estimate the molecular orientation through the measurement of optical anisotropy,[27] but there appear to be no examples about water as yet.

In this situation we have executed the MD simulation to clarify the nature of liquid–vapor interface of water. We present in this paper the thermodynamic (static) quantities varying with temperature and orientational ordering of molecules near the surface. In Sec. II, we briefly give the thermodynamic and statistical mechanical formulas we used. The details of the computer simulation technique are described in Sec. III, and the results, including density profiles, surface tensions, and orientational distribution functions, are in Sec. IV. These are discussed in Sec. V in more detail, being compared with the LJ system and also with the experimental results of surface potential measurement and ellipsometry. Section VI is devoted to the conclusion.

II. THERMODYNAMICS

The aim of this section is to give the thermodynamic formulas used in this paper, so the readers may refer to other textbooks[2,18–20] for more general descriptions of the interfacial systems.

Assume that N particles are interacting with each other in a cell of volume V at temperature T and that this system is not uniform, but has a (liquid–vapor) interface of area A, i.e., the state point of the system is on the coexistence line. The following conditions define the volume of liquid phase V_l and that of vapor phase V_v:

$$V = V_l + V_v, \quad N = n_l V_l + n_v V_v , \tag{1}$$

where n_l and n_v are the number density of bulk liquid and vapor, respectively. In other words, Eq. (1) determines the Gibbs surface. Then it is generally impossible to represent other thermodynamic quantities as a simple sum of those of bulk phases, but one needs to add the "surface term," which is proportional to the surface area A. For example, the internal energy U, the Helmholtz free energy F, and the entropy S are represented as follows:

$$U = u_l V_l + u_v V_v + u_s A, \quad F = f_l V_l + f_v V_v + f_s A , \tag{2}$$

$$S = s_l V_l + s_v V_v + s_s A,$$

where u_l is the energy density of bulk liquid, u_v that of bulk vapor, u_s the so-called "surface excess energy," etc. These quantities of lower case letter are dependent only on the temperature T, considering that the system is in the coexistent state. The following thermodynamic relation is easily obtained:

$$f_s = u_s - T s_s . \tag{3}$$

Next let us consider virtual expansion of the area A with the volume and the temperature fixed. The force acted in this process, the so-called "surface tension" γ, is equal to the work W (or the free energy change) needed for the expansion by unit area

$$\gamma = \frac{dW}{dA} = \left(\frac{\partial F}{\partial A}\right)_{v,T,N} = f_s . \tag{4}$$

The derivative of γ with respect to T gives s_s:

$$\frac{d\gamma}{dT} = -s_s . \tag{5}$$

Experimentally, γ is almost the sole measurable quantity, so one uses Eq. (5) to obtain s_s and then Eq. (3) to estimate u_s. In computer simulation study, however, both γ and u_s are easily calculated, so we can obtain s_s without differentiation of γ with T, which would need exhaustive computational resources because one must obtain precise values of γ for numerical differentiation. As far as we noticed, the usefulness of Eq. (3) to evaluate the interesting and important quantity s_s is not so widely recognized. We will show in Sec. IV how well this relation works.

To calculate γ by computer simulation, the following "virial expressions"[28] is convenient:

$$\gamma = \frac{1}{2}\int_{-\infty}^{\infty} dz_1 \int d\,\mathbf{\Omega}_1\, d\mathbf{r}_2\, d\,\mathbf{\Omega}_2\, \rho^{(2)}(\mathbf{r}_1,\mathbf{\Omega}_1,\mathbf{r}_2,\mathbf{\Omega}_2)$$

$$\times\left[\frac{1}{2}\left\{x_{12}\frac{\partial}{\partial x_{12}} + y_{12}\frac{\partial}{\partial y_{12}}\right\} - z_{12}\frac{\partial}{\partial z_{12}}\right] u(\mathbf{r}_1,\mathbf{\Omega}_1,\mathbf{r}_2,\mathbf{\Omega}_2)$$

$$= \int_{-\infty}^{\infty} dz\left[-\tfrac{1}{2}\{P_{xx}(z) + P_{yy}(z)\} + P_{zz}(z)\right]$$

$$= \int_{-\infty}^{\infty} dz\left[-P_t(z) + P_n(z)\right] , \tag{6}$$

where $\rho^{(2)}$ is the two-body distribution function, u is the pair potential ($\mathbf{r}_i$ and $\mathbf{\Omega}_i$ are the position and the orientation of the ith molecule, respectively), P_{ii} ($i = x,y,z$) is the pressure tensor, P_n is the pressure normal to the surface, and P_t is the tangential pressure. We assume here for simplicity that the interface is a plane normal to the Z axis. The definition of the local pressure tensor is according to Harashima[29] here, but the result after integration with respect to z is independent of definition.

III. COMPUTER SIMULATION

A. Simulation of water

One of us (YK) recently reported[30] the equation of state of fluid water with the Carravetta–Clementi (CC)[31] pair potential by the MD simulation technique. There the CC water system is found to reproduce the nature of real water semiquantitatively and the equation of state is given in an analytical form, from which one can easily get the liquid–vapor coexistence line. Therefore, we also used the CC potential here to utilize the equation of state to check our results.

The MD program was almost the same as before, which is based on MDMPOL of Smith and Fincham,[32] but was improved with tabulation and second order interpolation technique of some mathematical functions (EXP, SQRT, and ERFC). The stress tensor was calculated with formula (A8) of Nosé and Klein's paper,[33] represented in Ewald summation form.

The simulation cell (see Fig. 1) is a rectangular prism of dimensions $L_x = L_y = 32.5$ Å and $L_z = 120$ Å, in the middle of which we placed 1000 water molecules interacting with the CC potential. We adopted a complete periodic boundary condition (PBC) rather than the usual periodicity of only X and Y directions, because the Ewald summation technique is easily applied for the complete periodicity. The radius of the short-ranged potential cutoff is 12 Å, which is larger than the usual one; instead we did not add the long-tail correction because the evaluation of the correction was difficult for such inhomogeneous systems as this. The liquid layer exists between about 40 and 80 Å and the interference of liquid layers due to the complete PBC is found to be negligible. There was no external field potential in our simulation, but the liquid layer was found to be stable and did not resolve into small clusters in the temperature range we calculated (Table I), the reason for which may be the periodicity of the X and Y directions. Other simulational conditions are also listed in Table I; the critical temperature T_c of CC water is near 603 K,[30] but the triple point temperature T_t is not known (we guess it exists between 250 and 275 K, though). The total energy conservation is quite well, within $\pm 0.01\%$. The CPU time is 0.5–0.8 s/step (varying with the density of liquid phase) on FACOM VP-200 vector processor at Kyoto Univeristy Data Processing Center.

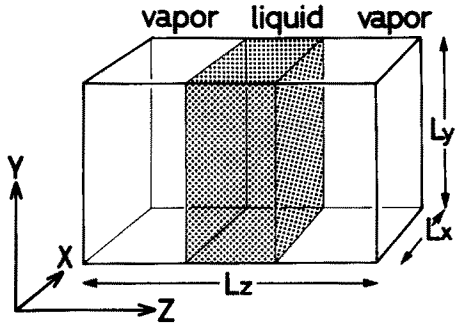

FIG. 1. The simulation cell.

The initial configuration is the lattice of cubic ice I_c. After the equilibrating process of 10 000 steps (5 ps) at 400 K, we started sampling and averaging. To get lower temperature samples, we cooled gradually the system of higher temperature and annealed it for about 5000–7000 steps. Sampling was repeated several times and the error estimation was done by comparing these results.

B. Simulation of the Lennard-Jones system

In order to investigate the difference of the nature of the interface of water from that of simple fluids, we also executed MD simulation of the liquid–vapor interface of the LJ system. The interaction potential $u(r)$ is

$$u(r) = 4\epsilon\{(\sigma/r)^{12} - (\sigma/r)^6\}, \tag{7}$$

where the particle diameter $\sigma = 3.405$ Å and the potential depth $\epsilon = 119.8$ K are those for Ar.[34] The simulation cell is similar to that used for water, but the size is $L_x = L_y = 32$ Å and $L_z = 90$ Å. The number of particles is 1000 and the complete PBC is also adopted. The cut-off radius is 15 Å. Other simulation conditions are given in Table I; notice that T_t is 79 K.[34] The CPU time is about 0.1 s/step on FACOM VP-200. Starting from the fcc lattice and after equilibrating the system at $T = 120$ K for 10 000 steps (50 ps), the data were samples and averaged. For other temperatures, the gradual cooling and annealing was repeated.

TABLE I. Simulation condition and some results for the water system and the Lennard-Jones system; averaged kinetic energy ⟨KE⟩, bulk liquid density ρ_l obtained from parameter fitting, and pressure P of the system.

System	Setting temperature (K)	Step size (10^{-15} s)	Number of steps	⟨KE⟩ (K)	ρ_l (g cm^{-3})	P (MPa)
Water	400	0.5	15 000×3	405.2 ± 1.0	0.7564 ± 0.0006	−2.38 ± 0.91
	350	0.5	16 000×3	351.5 ± 0.5	0.8196 ± 0.0005	−3.98 ± 0.77
	300	0.5	14 000×3	299.7 ± 1.0	0.8599 ± 0.0004	−6.20 ± 0.29
	275	0.6	13 000×4	276.7 ± 1.7	0.8678 ± 0.0005	−8.07 ± 1.20
	250	0.7	13 000×6	248.8 ± 1.9	0.8736 ± 0.0006	−7.33 ± 2.89
LJ	120	5.0	30 000×3	118.90 ± 0.42	1.1506 ± 0.0016	1.180 ± 0.085
	100	6.0	30 000×6	100.55 ± 1.03	1.2904 ± 0.0014	0.335 ± 0.045
	80	8.0	30 000×5	79.96 ± 0.17	1.4174 ± 0.0021	0.022 ± 0.020

IV. RESULTS

A. Profiles and parameter fitting

The averaged temperature T (kinetic energy), the pressure, and the bulk liquid density ρ_l of the system are tabulated in Table I (ρ_l is obtained by parameter fitting, see below). The state points are well on the coexistence line, which is in Ref. 30 for CC water and in Ref. 34 for the Lennard-Jones system.

To begin with, we show the one-body distribution function $\rho(z)$, the so-called "density profile," and the local potential energy function $u(z)$, the "energy profile." We divided the cell into layers of thickness 2 Å for water, 1 Å for LJ, and statistically averaged the density or the potential energy of the layers; it is better to adopt thinner layers, say 0.2 Å, to obtain more detailed data, but much more computation would be required to get meaningful statistical average. Strictly speaking, the definition of $u(z)$ is not unique; the problem is where we count the pair potential energy $u(\mathbf{r}_1,\mathbf{r}_2)$ between particles 1 and 2, that is similar to the case of virial calculation.[19] We arbitrarily divided u into halves and counted them on $\mathbf{r}_1$ and $\mathbf{r}_2$, like Harashima's treatment of virial; however, this does not affect the calculation of the surface excess quantities in the following subsection because such quantities are obtained after integration of $u(z)$ with respect to z.

The data are parameter fitted to some analytical functions. For density profile, three functional forms have been proposed[3]; the hyperbolic tangent (tanh, or the Fermi) type,[35] the Fisk–Widom type,[36] and the error-function type.[37] The difference among these three becomes larger near the critical point, but within the temperature range we studied here these functions give almost the same results, so hereafter we adopt the tanh profile, which is the most tractable. For the energy profile, though it does not seem as yet that there exist definite functions, we also adopt the tanh profile. We used the program SALS for nonlinear least-square fitting developed by Oyanagi *et al.*[38] The functional forms are as follows;

$$\rho(z) = \tfrac{1}{2}(\rho_l + \rho_v) + \tfrac{1}{2}(\rho_l - \rho_v)\tanh[(z - Z_{d0})/2\delta_d], \tag{8}$$

$$u(z) = \tfrac{1}{2}(u_l + u_v) + \tfrac{1}{2}(u_l - u_v)\tanh[(z - Z_{u0})/2\delta_u],$$

where the quantities with l (for liquid) and v (for vapor) are those of the bulk phases, Z_0 is the position of the middle of the transition layer, and δ is the parameter for thickness of the interface; for the tanh profile, the usual "10–90 thickness" t is related to δ as $t = 4.394\,\delta$.

The parameters as the results of fitting are listed in Table II. Generally speaking, the thickness t and the position Z_0 of the density profile differ from those of energy profile. For Z_0, the energy surface is always inner, or in the liquid side for both water and LJ. This is easily understood if we remember that the local potential energy is in proportion not to the local density itself, but quite roughly, to the square of it. For t, however, the two systems behave in a different man-

TABLE II. Parameter-fitting results of density profile and energy profile; the hyperbolic tangent function is assumed, see Eq. (8). ρ's and u's are the density and the potential energy of bulk phases (liquid and vapor), respectively, t's are the 10–90 thicknesses, and Z_0's are the positions of the Gibbs surface; there are two surfaces (left and right) in our cell (see Fig. 1). The molecular diameter σ is 2.641 Å for water (Ref. 37) and 3.405 Å for Lennard-Jones system.

Density profile	System	T (K)	ρ_l (g cm^{-3})	ρ_v (g cm^{-3})	t_d (Å)	t_d (σ)	Z_{d0} (Å) (left)	Z_{d0} (Å) (right)
	Water	400	0.7564	0.0022	7.989	3.02	40.459	77.997
		350	0.8196	0.0009	5.771	2.19	42.098	76.518
		300	0.8599	0.0004	5.148	1.95	42.726	75.664
		275	0.8678	0.0000	3.614	1.38	43.033	75.356
		250	0.8736	0.0001	3.560	1.35	42.905	75.370
	LJ	120	1.1506	0.0593	10.668	3.13	16.808	71.312
		100	1.2904	0.0136	8.148	2.39	18.323	68.104
		80	1.4174	0.0004	5.450	1.60	20.480	66.234

Energy profile	System	T (K)	u_l (kJ cm^{-3})	u_v (kJ cm^{-3})	t_u (Å)	t_u (σ)	Z_{u0} (Å) (left)	Z_{u0} (Å) (right)
	Water	400	−1.3239	0.0001	7.042	2.67	41.171	77.316
		350	−1.5954	0.0001	6.020	2.28	42.689	76.004
		300	−1.8223	0.0001	4.764	1.80	43.110	75.198
		275	−1.9094	0.0001	3.966	1.50	43.386	75.032
		250	−2.0101	0.0000	3.301	1.25	43.006	75.223
	LJ	120	−0.1352	0.0005	10.811	3.18	18.960	69.171
		100	−0.1739	0.0008	8.965	2.63	20.271	66.083
		80	−0.2154	0.0004	7.239	2.13	21.996	64.582

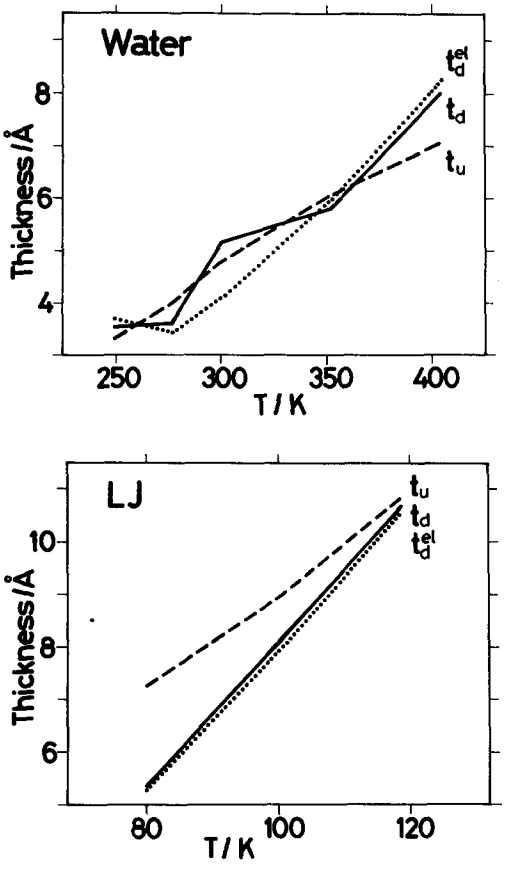

FIG. 2. The temperature dependence of the surface thicknesses t_d (from density profiles, solid lines), t_u (from energy profiles, dashed lines), and t_d^{el} (from ellipticity coefficients, dotted lines, see Sec. V D) for (a) water and (b) Lennard-Jones system.

ner as is seen in Fig. 2; t_d and t_u are almost the same for water, but t_d is much smaller than t_u for LJ, especially near the triple point. The reason is not precisely understood, but this phenomenon suggests that the liquid–vapor interface of water is energetically very sharp in comparison with the simple fluid, and that some ordering of water molecules occurs to lower the potential energy.

For the reduced thickness t_d/σ, that of water is a little less than that of LJ(Table II). It is said from elipsometric experiments[3] that the thickness of water surface ($t_d/\sigma \sim 1$) is much smaller than that of other liquids ($t_d/\sigma \sim 2$), but one cannot find such a remarkable tendency from our simulational results. One probable explanation of the ellipsometric result is the misfit of the density profile with the tanh function. This point will be discussed in more detail in Sec. V, but is clearly seen in Fig. 3, where both profiles and the tanh functions are represented in reduced units; $Z^* = (Z - Z_0)/\sigma$, $\rho^* = \rho N_A \sigma^3/M$, and $u^* = u\sigma^3/k_B\epsilon$ (N_A is the Avogadro's number, M is molecular weight, k_B is the Boltzmann constant). In particular, near the liquid side of the surface, the density seems to be higher than that of the bulk liquid, which suggests the existence of some structural change.

It is also seen in Fig. 3 that the middle of the system (the right side of the figure) is completely bulk liquid, so the two surfaces in the simulation cell (right and left) do not appear to interfere with each other; remember that the cut-off radius is 12 Å (or 4.54 in reduced unit) for water and 15 Å (or 4.41) for LJ, respectively.

Recently Braslau *et al.*[24] executed the x-ray reflectivity measurement of water and reported the "surface roughness" $\langle u^2 \rangle = 3.24 \pm 0.05$ Å at $T = 25$ °C. Since $\langle u^2 \rangle$ can be interpreted as the mean-square amplitude for capillary waves,[24] the 10–90 thickness t_d is related to it as $t_d = 2.563\langle u^2 \rangle$. Therefore their result gives $t_d = 8.304 \pm 0.128$ Å, which is much larger than our result 5.148 Å. One of the reasons for this disagreement is the suppression of capillary waves due to the finite size of the simulation cell.

B. Surface excess quantities

Next we use the results of parameter fitting described above and the thermodynamic relations [Eqs. (2) and (3)] to obtain the surface excess energy u_s and the surface excess entropy s_s. Since we assume the tanh-type profiles, one can calculate u_s analytically from Eq. (2) as follows:

$$\begin{aligned} u_s &= \int_{-\infty}^{\infty} u(z)dz - \left[\int_{-\infty}^{z_{d0}} u_v dz + \int_{z_{d0}}^{\infty} u_l dz\right] \\ &= \frac{u_l - u_v}{2}\left[\int_{-\infty}^{z_{d0}} \left\{1 + \tanh\frac{z - Z_{u0}}{2\delta_u}\right\}dz \right. \\ &\quad \left. + \int_{z_{d0}}^{\infty}\left\{-1 + \tanh\frac{z - Z_{u0}}{2\delta_u}\right\}dz\right] \\ &= (u_l - u_v)\cdot(Z_{d0} - Z_{u0}). \end{aligned} \tag{9}$$

This formulation suggests that the accuracy of calculation depends mostly on the precision of $Z_{d0} - Z_{u0}$. The s_s is evaluated from Eq. (3). The results are listed in Table III. The last column is the molar surface entropy defined by Good[1] as follows:

$$sA = 1.10 \times (M/\rho_l)^{2/3} N_A s_s , \tag{10}$$

where 1.10 is a factor reflecting the way of packing of liquid. A detailed discussion about this quantity is given later in Sec. V B.

For the surface tension of water, an analytical functional form fitted to experimental data is given by Vargaftik *et al.*[23] In Fig. 4, our results and the ones calculated from their empirical formula are compared. The simulated γ and u_s are only half of the experimental values, but s_s is nearly the same with the experimental result; the reason is probably that the energy and the free energy are strongly dependent upon the density (notice that the density of the bulk liquid of CC water coexisting with its vapor is lower by about 15%–25% than that of real water), but that the entropy, the quantity reflecting the structure, is less dependent on it. For the LJ system, γ is in accordance with the figure in Ref. 2, but there is a little discrepancy for u_s, especially near T_t. The accuracy is, however, quite good, so Eq. (3) proves to be very useful to estimate the surface excess entropy.

As is well known, one of the "abnormal characters" of the water surface is the fact that the excess entropy s_s lowers[2] as the temperature decreases to T_t. This is clearly shown in Fig. 4. On the other hand, s_s hardly changes near T_t for the

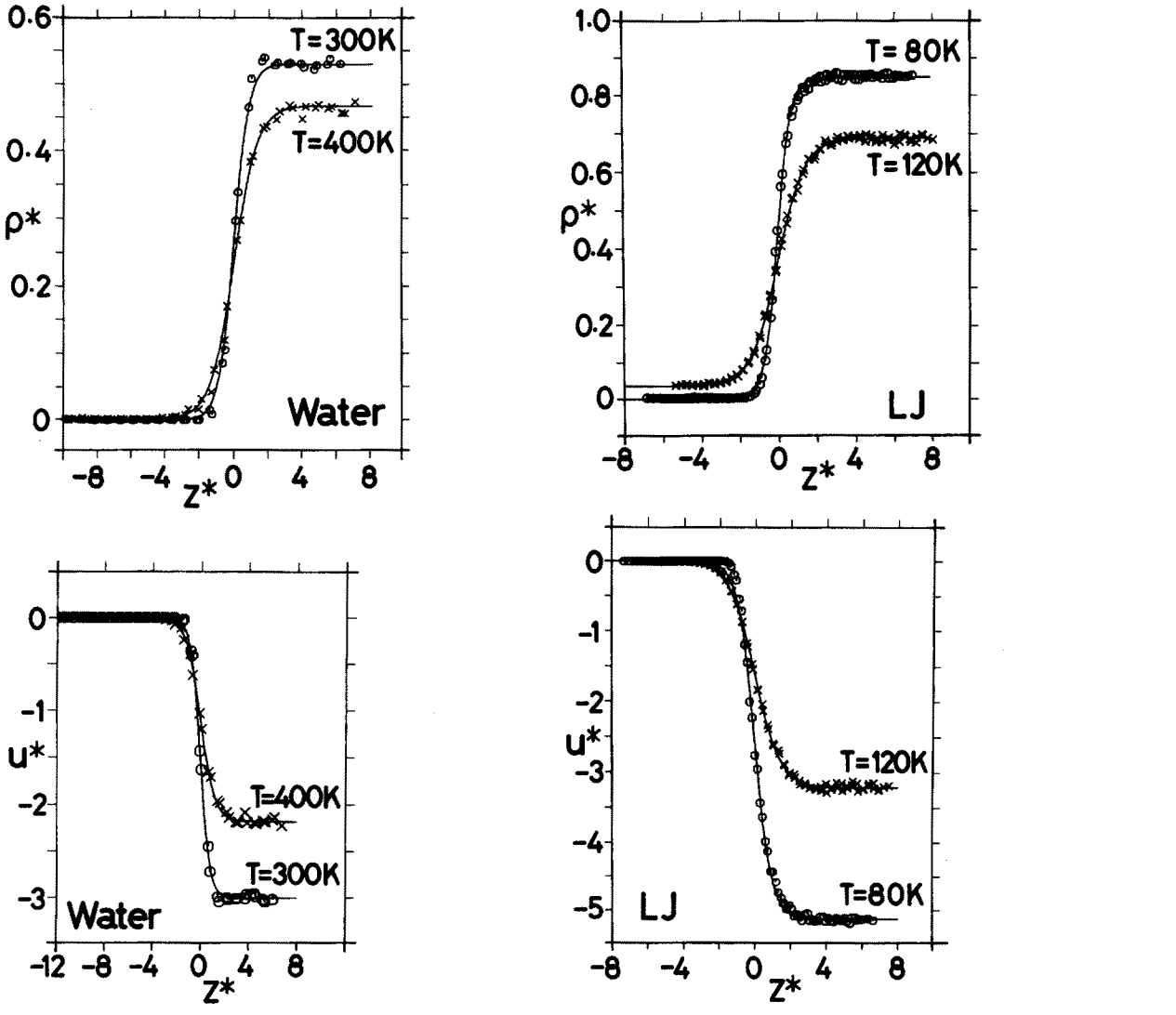

FIG. 3. The density profile $\rho^*(z^*)$ and the energy profile $u^*(z^*)$ in reduced units; solid lines are tanh functions least-square fitted to simulation data; LJ parameters for reduced units are $\sigma = 2.641$ Å and $\epsilon = 809.1$ K for water (Ref. 37), $\sigma = 3.405$ Å and $\epsilon = 119.8$ K for LJ(Ar).

LJ system (see Table III). Here again, the existence of some structural ordering of water surface near T_t is suggested. Moreover, the similar suggestion is offered when we look upon the temperature dependence of u_s; that of water rapidly decreases as the temperature decreases, i.e., some stabilization of energy occurs, but the LJ system does not show such tendency. A rather simple cluster model of water may give the reasons for these phenomena, as proposed by Luck.[40]

C. Orientational structure

In order to investigate the orientational ordering of water near the surface, we define two angle variables (Fig. 5); the angle between the dipole of the molecule (the C_2 axis, from the O atom to the M site[31]) and the space-fixed Z axis (from the liquid side to the vapor side) θ and the rotational angle around the C_2 axis ϕ; ϕ is defined to be 90° when the line connecting two H atoms is parallel to the X–Y plane, or the surface. Owing to the symmetry of the molecule and the system, the range of the variables is $0° \leqslant \theta \leqslant 180°$ and $0° \leqslant \phi \leqslant 90°$, respectively.

First, we show the statistical average of them, $\langle\theta\rangle$ and $\langle\phi\rangle$, as functions of the position z in Fig. 6. At higher temperatures ($T = 400$ or 350 K), one cannot see any deviations from random orientation; notice that the complete randomness gives $\langle\theta\rangle = 90°$ and $\langle\phi\rangle = 45°$ by definition. At lower temperatures ($T \leqslant 300$ K), there is a small deviation; $\langle\theta\rangle < 90°$ and $\langle\phi\rangle < 45°$, which means the preference for the orientation of the molecule with its one H atom projecting towards the vapor.

To look upon it in more detail, we drew contour maps of (θ,ϕ) distribution (examples at $T = 300$ K are shown in Fig. 7). It is found that there are two typical orientations (Fig. 8) which water molecules take near the surface. In the vapor side, the peak of the distribution exists around $\theta \sim 50°$ and $\phi \sim 0°$, which means that the water molecule is projecting its one H atom to the vapor phase as was observed in the results of $\langle\theta\rangle$ and $\langle\phi\rangle$. On the other hand, in the liquid side the peak

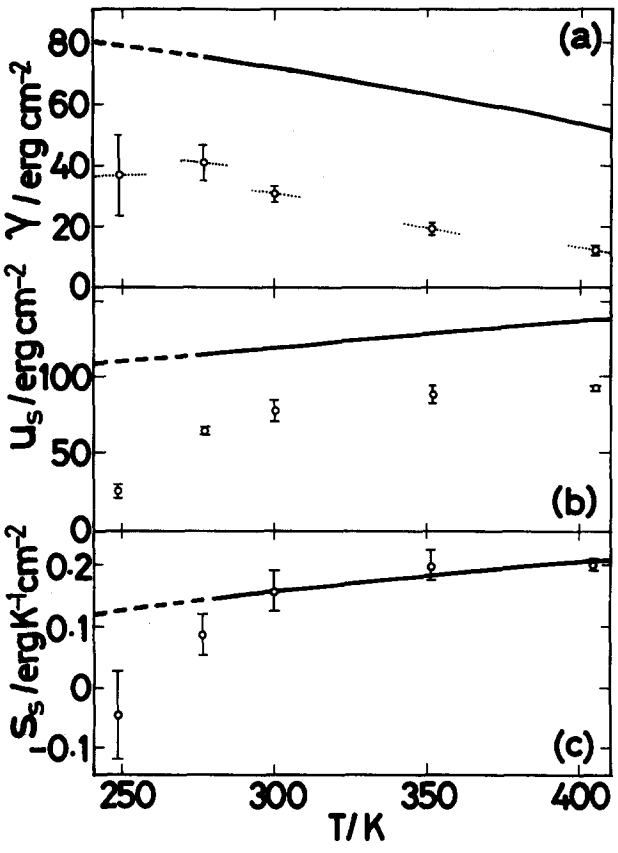

FIG. 4. The surface excess quantities of CC water compared with the experimental data (Ref. 21) (solid lines); (a) surface tension γ (excess Helmholtz free energy); (b) excess internal energy u_s, and (c) excess entropy s_s. The dotted lines are temperature derivative of the surface tension calculated from Eq. (4).

being around $\theta \sim 110°$ and $\phi \sim 90°$ suggests that the molecule prefers to lie down on the surface with its two H atoms slightly projected into the liquid phase. The latter tendency of orientation continues rather deeper into the liquid phase, say about 10 Å. Croxton's estimation[14] is in accordance with the vapor-side orientation, and Stillinger and Ben-Naim's one[12] corresponds to the liquid-side orientation. Since the local density of the liquid side is much higher than that of the vapor side, the "lying-down" orientation plays a more important role in considering various interfacial phenomena, such as the surface potential and ellipticity coefficient, as seen later in Sec. V.

At higher temperatures ($T = 400$ and 350 K), these orientational tendencies are weakened, as is easily understood. At lower temperatures ($T = 275$ and 250 K), however, the orientational ordering is not developed so much, contrary to our expectation. The reason may be partly because the transition layer becomes so thin that the almost opposite tendencies of orientation are not observed separately; notice that we statistically averaged the orientational distribution every 2 Å and the surface thickness $t \sim 3.5$ Å at these temperatures.

V. DISCUSSION

A. Surface potential

Water molecules have such a large dipole moment that one can expect that the orientational ordering of them makes the electrical double layer and causes the surface potential. Assume that molecules with dipole moment μ exist in a layer of thickness Δ. If its number density is n and the averaged orientation is $\langle \cos\theta \rangle$ (θ is defined as described in Sec. IV C), the following electric potential difference between both sides of the layer is generated:

$$\chi_\Delta = \frac{\Delta\mu}{\epsilon_0} n \langle \cos\theta \rangle , \tag{11}$$

where ϵ_0 is the dielectric constant of the vacuum. The summation, or the integral of χ_Δ gives the electric potential relative to its bulk liquid phase ($z = +\infty$) is expressed as follows:

$$\chi(z) = \frac{\mu}{\epsilon_0} \int_\infty^z dz \frac{\rho(z)}{M} \langle \cos\theta \rangle_z , \tag{12}$$

where $\rho(z)$ is the mass per unit volume and M is the molecular weight of water [so $\rho(z)/M$ is the profile of number density]. The surface potential χ is defined as the potential of the bulk liquid relative to its vapor

$$\chi = -\chi(-\infty) = \frac{\mu}{\epsilon_0} \int_{-\infty}^{\infty} dz \frac{\rho(z)}{M} \langle \cos\theta \rangle_z . \tag{13}$$

The μ of CC water is evaluated to be 7.082×10^{-30} C m = 2.12 D from the charges and bond lengths in Ref. 31; one of the experimental values is 1.855 D.[15] The result of the calculation is listed in Table IV. The positive values of χ

TABLE III. Surface excess thermodynamic quantities; surface tension γ, surface excess internal energy u_s, surface excess entropy s_s, and molar surface entropy sA defined in Eq. (10). R is the gas constant, 8.314 J K^{-1} mol^{-1}.

System	T (K)	γ (erg cm^{-2})	u_s (erg cm^{-2})	s_s (erg K^{-1} cm^{-2})	sA (R)
Water	400	11.7 ± 1.8	92.3 ± 2.1	0.199 ± 0.010	1.84 ± 0.09
	350	18.7 ± 2.3	88.2 ± 6.2	0.198 ± 0.024	1.74 ± 0.21
	300	30.5 ± 2.7	77.4 ± 7.5	0.156 ± 0.034	1.32 ± 0.29
	275	41.0 ± 6.2	64.6 ± 2.7	0.085 ± 0.033	0.72 ± 0.28
	250	36.7 ± 13.2	24.9 ± 4.6	−0.047 ± 0.072	−0.39 ± 0.60
LJ	120	5.89 ± 0.49	29.13 ± 0.08	0.195 ± 0.005	2.32 ± 0.06
	100	9.59 ± 0.83	34.68 ± 0.65	0.250 ± 0.015	2.50 ± 0.15
	80	14.34 ± 0.75	34.18 ± 1.47	0.248 ± 0.028	2.33 ± 0.26

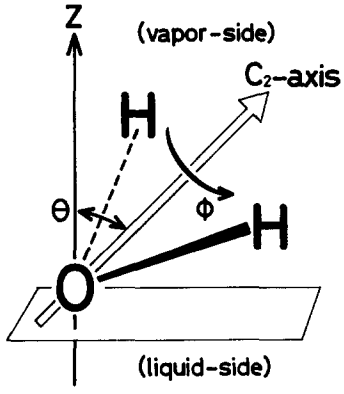

FIG. 5. The variables used to represent the orientation of a water molecule. ϕ is 90° when the straight line connecting both H atoms is parallel to the surface.

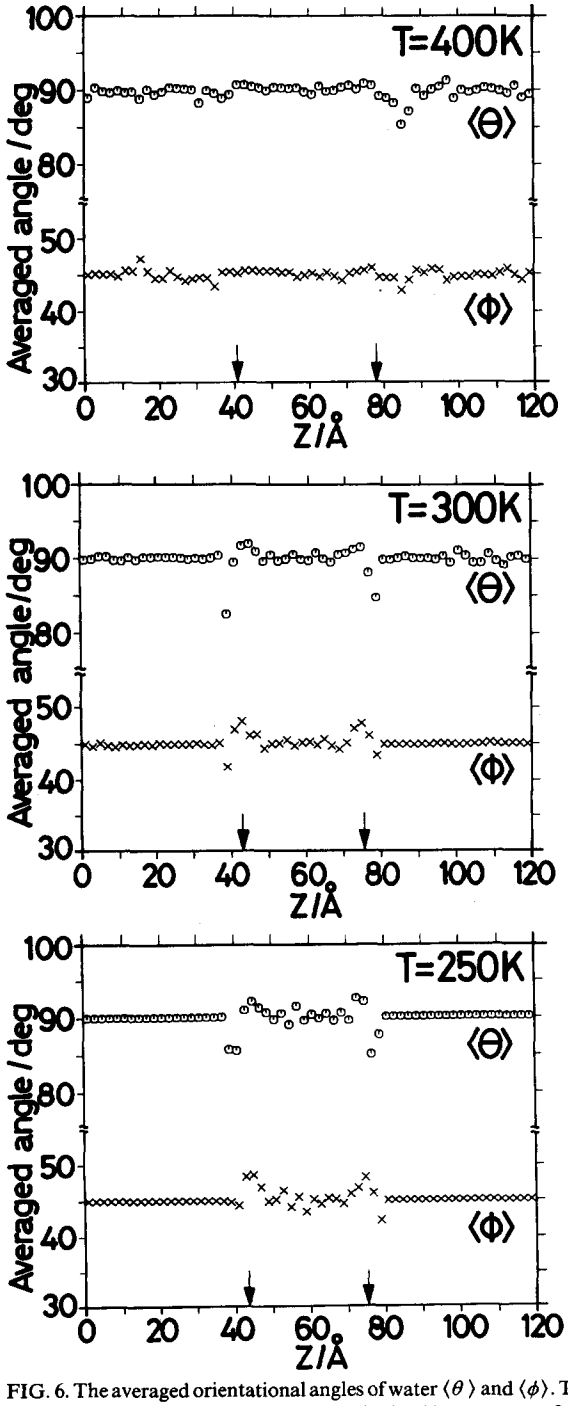

FIG. 6. The averaged orientational angles of water $\langle\theta\rangle$ and $\langle\phi\rangle$. The arrows show the position of the Gibbs surfaces, obtained by parameter fitting of the density profile.

mean that the dipole of water tends to point inwards (into the liquid side), but the detail is more complicated because there exist two different orientations, as suggested in Sec. IV C. It is shown in Fig. 9, an example of the local electric potential $\chi(z)$ calculated with Eq. (12); the inner (liquid) phase is certainly positive (relative to the vapor phase), but, as expected, the slight negative part exists in the vapor side of the transition layer, that corresponds to the orientation with one H atom projecting towards the vapor. The temperature dependence of χ is as expected from the result in Sec. IV C, i.e., as T increases, χ decreases rapidly, and at $T<300$ K χ seems to be saturated.

Experimentally, the evaluation of χ is an important problem in analytical chemistry and electrochemistry when one tries to divide the free energy of hydration of ions into "chemical" contribution due to short-range interactions and electrostatic contributions. The χ is not a directly measurable quantity, and one can only estimate it through subtracting the chemical free energy change, calculated from theoretical consideration based upon various solvation models, from the free energy change measured by such as the Kenrick–Frumkin method.[41] As a result of such model calculations, even the sign of χ has been long controversial[42] since Frumkin[43] gave the conclusion of $\chi\sim+0.1-+0.2$ V. Schiffrin[44] evaluated the temperature coefficient of χ and found $(d\chi/dT)=-0.39\pm0.04$ mV/K at $T=25$ °C, which suggests χ is positive (because χ is expected to be zero at T_c) and agrees qualitatively with our result. Conversely, the result of computer simulation can be used to estimate the validity of assumptions in calculating the chemical contribution of the ionic hydration.

B. Entropy lowering

Good[1] collected surface entropy data of various materials near T_t, including water, and proposed that the molar surface entropy sA [defined in Eq. (10)] can be taken as a criterion of surface orientation. He showed that the averaged sA of nonpolar compounds is 24.4 J/K mol ($=2.93\ R$, where R is the gas constant), that of polar nonhydrogen bonding compounds is 23.8 J/K mol ($=2.86\ R$), but that of strongly hydrogen bonded ones (water, methanol, etc.) is 10.8 J/K mol ($=1.30\ R$). From Table III, it is found that the results of our simulations agree quite well with Good's statement; sA is 1.3 R for water at $T=300$ K and 2.5 R for LJ at $T=100$ K.

Good tried to explain this "entropy lowering" of $2.9-1.3\ R=1.6\ R$ by considering a deficit of entropy due to the completely oriented n layers as follows:

$$\delta s = nR\ln 2\,. \tag{14}$$

His result of $\delta s=1.6\ R$ gives the number of oriented layers $n\sim2.3$, from which he suggested that the orientational ordering continues at least deep into the third layer. Can this picture explain our simulational results? In order to estimate the entropy deficit of the orientational ordering, we calculated the "one-body excess entropy" ΔS^1, defined with the (θ,ϕ)-distribution function $P(\theta,\phi;z)$ as

$$\Delta S^1=\int_{-\infty}^{\infty} dz\Delta s^1(z)\,,$$

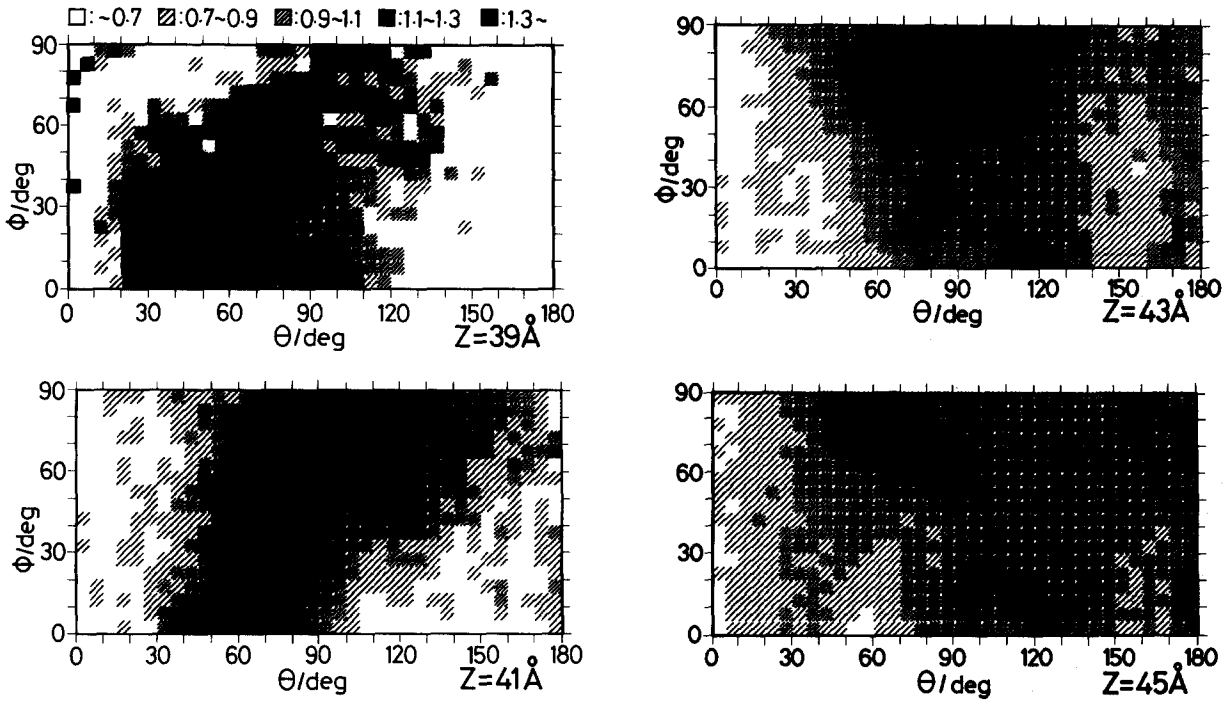

FIG. 7. Contour maps of (θ,ϕ) distribution of water at $T = 300$ K, normalized to unity if the orientation is completely random; the ranges corresponding to the various shades are described above the first figure. The position of the Gibbs surface is $Z = 42.7$ Å.

$$\Delta s^1(z) = -\frac{\rho(z)}{M} k_B \int\int d\theta\, d\phi \{P(\theta,\phi;z)\ln P(\theta,\phi;z) - P_0 \ln P_0\}$$

$$= -\frac{\rho(z)}{M} k_B \langle \ln P(\theta,\phi;z)\rangle - \langle \ln P_0\rangle\}, \qquad (15)$$

where $\rho(z)/M$ is the local number density and P_0 is the uniform distribution. In Fig. 10 an example of the local excess entropy $\Delta s^1(z)$ is shown at $T = 300$ K. The lowering of entropy certainly occurs near the surface, but is also observed in the bulk due to the statistical fluctuation of $P(\theta,\phi;z)$. To remove this fluctuation, we further estimated the "bulk entropies (of liquid and vapor)" from the local entropy and subtracted them from the value of the integration. The results are shown in Table V, where the total decrease of the excess entropy from that of $T = 400$ K, ΔS, is also listed. One can see that the contribution of the one-body term is by an order of magnitude smaller than the total decrease. Therefore Good's simple explanation of entropy lowering by dipole-orientational ordering cannot be accepted and the importance of many-body effects (more complicated structure due to the hydrogen bonded network, etc.) is suggested.

The detail of this is not known yet, but the phenomena analogous to the hydrophobic structure making[45] probably occur. For example, ΔS_h (the hydration entropy) of apolar solutes at 25 °C is about -240 to -130 J/K mol (-29 to -15 R),[45] which is consistent with our result of $\Delta SA = -2R$ to $-R$ (Table V) of the liquid–vapor interface if one regards the vacuum as a solute and assumes that about 10 water molecules are in contact with one solute; notice that ΔS_h is the entropy per mole of solute and ΔSA is per mole of water.

C. Invariants

Egelstaff and Widom[46] discussed the possibility that the product of the isothermal compressibility κ and the surface tension γ of a liquid near its triple point is a fundamental

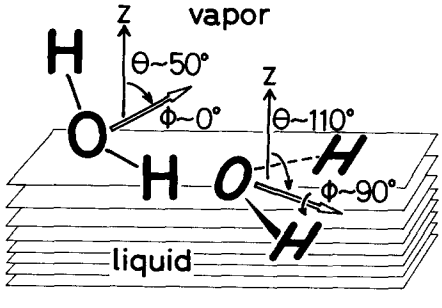

FIG. 8. Two typical orientations of water molecules near the surface.

TABLE IV. Surface potential χ of water. There are two surfaces (left and right) in our simulation cell (see Fig. 1) and the average of these values is given in the last column.

	χ (V)		
T (K)	(left)	(right)	(average)
400	0.043	−0.026	0.009
350	0.092	0.111	0.102
300	0.171	0.153	0.162
275	0.153	0.166	0.160
250	0.138	0.196	0.167

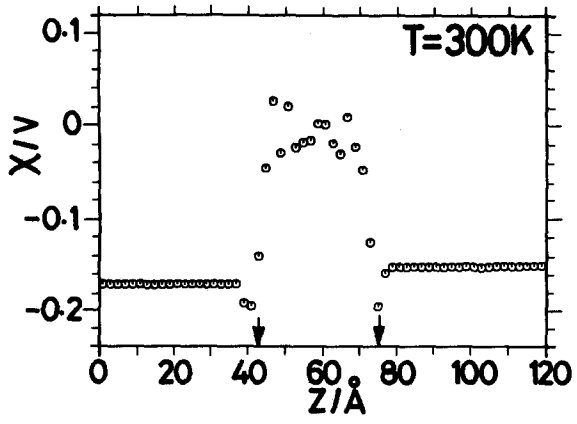

FIG. 9. The electric potential function $\chi(z)$ of water relative to its bulk liquid at $T = 300$ K, see Eq. (12); the value at $Z = 60$ Å is defined to be zero. The arrows show the position of the Gibbs surfaces.

length characteristic of the liquid. They showed data of various liquids and concluded that the value of $L = \kappa\gamma/0.07$ is about 4 Å, which would correspond to the surface thickness or the core diameter. More recently, Sanchez[47] progressed their theory and presented a new relation as follows:

$$\gamma(\kappa/\rho_l)^{1/2} = A_0^{1/2} \sim 0.26(\epsilon\sigma^2/M)^{1/2}, \tag{16}$$

where ϵ and σ are the LJ potential parameters for the liquid. We here study the applicability of these relations to our simulational results. For κ, we utilized the analytical form of the equation of state, for water in Ref. 30 and for LJ in Ref. 48. The results are listed in Table VI. The temperature dependence of L for water is much different from that for LJ; as T decreases to T_t, L of water increases rapidly, but L of LJ decreases slightly to the prediced value σ. The similar difference between water and LJ exists in the behavior of A_0 of Sanchez. From Eq. (16) $A_0^{1/2}$ should be equal to 4.19 for water ($\epsilon = 809.1$ K, $\sigma = 2.641$ Å, and $M = 18.015$)[39] and 1.40 for LJ ($\epsilon = 119.8$ K, $\sigma = 3.405$ Å, and $M = 39.95$). Relation (16) holds well for all simulated temperatures of the LJ system, but it is not so good for water and a strong temperature dependence is observed, as moderately stated by Sanchez.[47]

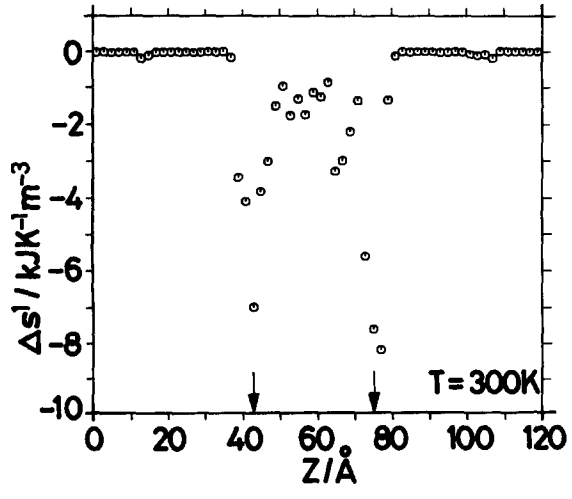

FIG. 10. The local one-body excess entropy $\Delta s^1(z)$ of water at $T = 300$ K, see Eq. (15); the arrows show the position of the Gibbs surfaces.

TABLE V. The decrease of entropy due to the orientational ordering of a water molecule. ΔS^1 is the one-body excess entropy defined by Eq. (15) and ΔS is the difference between s_s at that temperature and s_s at $T = 400$ K. A is the molar area similar to the one in Eq. (10).

T (K)	ΔS^1 (erg K^{-1} cm^{-2})	$\Delta S^1 A$ (R)	ΔS (erg K^{-1} cm^{-2})	ΔSA (R)
400	-0.0025 ± 0.0005	-0.023	0	0
350	-0.0038 ± 0.0001	-0.033	-0.001	-0.10
300	-0.0085 ± 0.0002	-0.072	-0.043	-0.52
270	-0.0058 ± 0.0002	-0.049	-0.114	-1.12
250	-0.0030 ± 0.0003	-0.025	-0.246	-2.23

D. Ellipsometry

Ellipsometry is the technique which measures the polarization of the light reflected at the interface.[49,50] Under certain assumptions one can obtain the information of the interface, such as its thickness and the dielectric constant. The coefficient of ellipticity $\bar{\rho}$, the value of the imaginary part of the ratio of the p and s reflection amplitudes at the Brewster angle, can be represented to the first order with the dielectric constant of the transition layer $\epsilon(z)$ as follows[49]:

$$\bar{\rho} = \frac{\pi}{\lambda} \frac{\sqrt{\epsilon_v + \epsilon_l}}{\epsilon_v - \epsilon_l} \eta_0 \tag{17}$$

and

$$\eta_0 = \int_{-\infty}^{\infty} dz \frac{[\epsilon(z) - \epsilon_v][\epsilon(z) - \epsilon_l]}{\epsilon(z)}, \tag{18}$$

where λ is the wavelength of the incident light, ϵ_l and ϵ_v are the dielectric constant of bulk liquid and vapor, respectively. Recently, Lekner[27] generalized this formula to the case where anisotropy of $\epsilon(z)$ exists and derived the similar formula to Eq. (17), with η_0 replaced by

$$\eta = \int_{-\infty}^{\infty} dz \left\{ \epsilon_{\parallel}(z) + \frac{\epsilon_v \epsilon_l}{\epsilon_{\perp}(z)} - \epsilon_v - \epsilon_l \right\}, \tag{19}$$

where $\epsilon_{\perp}$ and $\epsilon_{\parallel}$ are the dielectric constant normal and parallel to the interface, respectively.

We calculated $\bar{\rho}$ using these formulas. The problem is how we evaluate $\epsilon(z)$ from the density profile $\rho(z)$. We adopt here the Clausius–Mossotti formula[51]

$$\frac{\epsilon(z)}{\epsilon_0} = \left[1 + \frac{8\pi}{3} \frac{\rho(z)}{M} \alpha\right] \Big/ \left[1 - \frac{4\pi}{3} \frac{\rho(z)}{M} \alpha\right], \tag{20}$$

where α is the molecular polarizability and ϵ_0 is the dielectric constant of the vacuum. Taking account of the anisotropy of the transition layer, we obtain the dielectric constant as a tensor form

$$\epsilon_{kj}(z)/\epsilon_0 = \left(\delta_{ik} - \frac{4\pi}{3} \frac{\rho(z)}{M} \bar{\alpha}_{ik}\right)^{-1} \left(\delta_{ij} + \frac{8\pi}{3} \frac{\rho(z)}{M} \bar{\alpha}_{ij}\right), \tag{21}$$

where δ_{ij} is the unit tensor (the Kronecker's delta). The molecular polarizability tensor $\bar{\alpha}_{ij}$, when orientationally averaged with the (θ,ϕ) distribution $P(\theta,\phi;z)$, becomes diagonal due to the rotational symmetry of the system around the normal of the surface

TABLE VI. The "invariants" of the liquid–vapor interface; L is defined by Egelstaff and Widom (Ref. 46) as $L=\kappa\gamma/0.07$, and $A_0^{1/2}$ is defined by Sanchez (Ref. 47) as $A_0^{1/2}=\gamma(\kappa/\rho_l)^{1/2}$, where κ is the isothermal compressibility (here calculated from the equation of state), γ is the surface tension, and ρ_l is the bulk liquid density. For water there are two types of the equation of state (Ref. 30), G-EOS and L-EOS, and both results are listed.

System	T (K)	κ (Pa^{-1})	γ (dyn cm^{-1})	ρ_l (g cm^{-3})	L (Å)	$A_0^{1/2}$ [(erg cm^2 $g^{-1})^{1/2}$]
Water	400	16.2×10^{-10} (G-EOS)	11.7	0.756	2.71	1.71×10^{-4}
		17.4×10^{-10} (L-EOS)			2.86	1.78×10^{-4}
	350	12.1×10^{-10} (G-EOS)	18.7	0.820	3.23	2.27×10^{-4}
		12.4×10^{-10} (L-EOS)			3.31	2.30×10^{-4}
	300	11.2×10^{-10} (G-EOS)	30.5	0.860	4.88	3.48×10^{-4}
		13.0×10^{-10} (L-EOS)			5.66	3.75×10^{-4}
	275	11.0×10^{-10} (G-EOS)	41.0	0.868	6.44	4.62×10^{-4}
		17.3×10^{-10} (L-EOS)			10.13	5.79×10^{-4}
	250	11.3×10^{-10} (G-EOS)	36.7	0.874	5.92	4.17×10^{-4}
		81.5×10^{-10} (L-EOS)			42.73	11.21×10^{-4}
LJ	120	68.5×10^{-10}	5.89	1.15	5.76	1.44×10^{-4}
	100	33.5×10^{-10}	9.59	1.29	4.59	1.55×10^{-4}
	80	17.5×10^{-10}	14.34	1.42	3.59	1.59×10^{-4}

$$\bar{\alpha}_{ij}=\begin{cases}\bar{\alpha}_{\parallel}, & \text{for } i=j=x \text{ or } y\\ \bar{\alpha}_{\perp}, & \text{for } i=j=z,\\ 0, & \text{otherwise}\end{cases} \tag{22}$$

where $\bar{\alpha}_{\parallel}$ and $\bar{\alpha}_{\perp}$ are the orientationally averaged molecular polarizability normal and parallel to the surface, respectively, calculated as follows:

$$\bar{\alpha}_{\parallel}=\frac{1}{2}\int\int d\theta\, d\phi P(\theta,\phi;z)\,[\alpha_{xx}\{\cos^2\theta\cos^2\phi+\sin^2\phi\}+\alpha_{yy}\{\cos^2\theta\sin^2\phi+\cos^2\phi\}+\alpha_{zz}\sin^2\theta\,], \tag{23}$$

$$\bar{\alpha}_{\perp}=\int\int d\theta\, d\phi\, P(\theta,\phi;z)\,[\alpha_{xx}\sin^2\theta\cos^2\phi+\alpha_{yy}\sin^2\theta\sin^2\phi+\alpha_{zz}\cos^2\theta\,],$$

where the Jacobian $\sin\theta$ is included in $P(\theta,\phi;z)$. Substituting Eq. (22) for Eq. (21), one can obtain the following expression:

$$\epsilon_{\parallel}/\epsilon_0=\left(1+\frac{8\pi}{3}\frac{\rho}{M}\bar{\alpha}_{\parallel}\right)\Big/\left(1-\frac{4\pi}{3}\frac{\rho}{M}\bar{\alpha}_{\parallel}\right),$$
$$\epsilon_{\perp}/\epsilon_0=\left(1+\frac{8\pi}{3}\frac{\rho}{M}\bar{\alpha}_{\perp}\right)\Big/\left(1-\frac{4\pi}{3}\frac{\rho}{M}\bar{\alpha}_{\perp}\right). \tag{24}$$

This is a generalization of the Clausius–Mossotti formula (20).

We adopted two ways to calculate $\bar{\rho}$; one is to use directly the simulational results of density profile and another is to apply the tanh function determined in Sec. IV A. The latter is only for the isotropic case (18). The molecular polarizability of water we used is the one experimentally determined by Murphy[52] for the light of $\lambda=5145$ Å; $\alpha_{xx}=1.528$, $\alpha_{yy}=1.415$, and $\alpha_{zz}=1.468\times10^{-24}$ cm^3 in electrostatic units. For LJ (Ar), we used the value[15] $\alpha=1.642\times10^{-24}$ cm^3.

The results are given in Table VII. First, the dielectric constant of the bulk liquid calculated with Eq. (20) is compared with the experimental value; the agreement is quite good, especially for LJ system. For water, the fact that the obtained density of bulk liquid is lower than that of the real system causes the disagreement of ϵ_l. The Clausius–Mossotti formula, however, appears to be well applicable to both systems. Next, three ellipticity coefficients are tabulated; the one calculated with the tanh fitting is very different from the other two, especially for water. The anisotropic effect, though it agrees with the picture of the lying-down orientation (notice that lying down means $\bar{\alpha}_{\perp}<\bar{\alpha}_{\parallel}$), is quite small and it may be difficult to detect it experimentally. For experimental results of ellipsometry, readers may refer to Ref. 25 for water and Ref. 54 for Ar. The thickness of the transition layer is often determined from $\bar{\rho}$ under the assumption that the dielectric function has some analytic form, e.g., linear, exponential, or hyperbolic tangent.[27] We here use the tanh function that is equivalent to assuming the density profile as the tanh type and calculate the 10–90 thickness $t_d^{\rm el}$ with the following formula[27]:

$$\bar{\rho}=\frac{\pi}{\lambda}\frac{t_d^{\rm el}}{4.394}\sqrt{\epsilon_v+\epsilon_l}\,\ln\frac{\epsilon_l}{\epsilon_v}. \tag{25}$$

The results are in the last three columns of Table VII and Fig. 2. For LJ, the parameter-fitting result t_d and this $t_d^{\rm el}$ are almost the same, which suggests the assumption of the tanh-type density profile is valid. For water, however, t_d differs much from $t_d^{\rm el}$; the latter is smoother with respect to temperature dependence than the former and is smaller near $T=300$ K. This is due to the misfit of the density profile to the tanh function, as previously stated. The abnormal smallness of the thickness which Beaglehole[3] suggests may be explained by this.

Another fact one can notice is the increase of $\bar{\rho}$ near $T=250$ K. Kizel'[55] studied various organic compounds by the ellipsometric technique and found the similar raise of $\bar{\rho}$ near the freezing point for several types of liquid. He considered this phenomenon as "preparation for solidification," which may hold true in the case of water.

TABLE VII. The dielectric constant of bulk liquid ϵ_l, the ellipticity coefficient $\bar{\rho}$ and the surface thickness t_d^{el}. (a) The ϵ_l is calculated with Eq. (20). (b) The experimental value of ϵ_l is estimated with third order extrapolation of the data (for $\lambda = 5893$ Å) in Ref. 53. The $\bar{\rho}$ is calculated from Eq. (17) with Eq. (18) assuming tanh-type density profile (c), or through numerical integration of Eq. (18) for the isotropic case (d), and numerical integration of Eq. (19) for the anisotropic case (e). The t_d^{el} is obtained from Eq. (25).

System	T (K)	ϵ_l/ϵ_0		$\bar{\rho}$			t_d^{el} (Å)		
		Calc.[a]	Obs.[b]	Iso. + Tanh[c]	Iso.[d]	Aniso.[e]	Tanh	Iso.	Aniso.
Water	400	1.553	1.716	7.80×10^{-4}	8.03×10^{-4}	8.00×10^{-4}	7.99	8.23	8.11
	350	1.609	1.750	6.15×10^{-4}	6.32×10^{-4}	6.27×10^{-4}	5.77	5.93	5.87
	300	1.645	1.774	5.79×10^{-4}	4.71×10^{-4}	4.63×10^{-4}	5.15	4.19	4.11
	275	1.653	1.780	4.51×10^{-4}	3.88×10^{-4}	3.81×10^{-4}	3.97	3.42	3.35
	250	1.658	1.780	4.08×10^{-4}	4.24×10^{-4}	4.18×10^{-4}	3.56	3.70	3.65
LJ	120	1.406	1.414	6.17×10^{-4}	5.95×10^{-4}	···	10.67	10.51	···
	100	1.463	1.475	5.55×10^{-4}	5.30×10^{-4}	···	8.15	7.95	···
	80	1.517	1.526	4.13×10^{-4}	3.92×10^{-4}	···	5.45	5.27	···

E. Orientational structure

The origin of the orientational ordering of water near the surface, in principle a result of the anisotropic interaction between molecules, can be sought in two different ways; one is the picture where the electric multipoles are interacting and the other is the one where the hydrogen bonding plays an important role. For the former, Gubbins and his coworkers,[56,57] and Tarazona and Navascués[58,59] have developed the perturbation theory and the integrodifferential theory for the liquid–vapor interface of simple polar fluids (e.g., the Stockmayer model), and found that dipoles (and quadrupoles also) have the effect to align the molecules; the preferred orientation is the one parallel to the surface at its liquid side and the one perpendicular at the vapor side. This conclusion qualitatively agrees with our result, though the effect of more higher-order multipoles will not be estimated so easily in these theories. For the hydrogen-bonding picture, Lee *et al.*[60] executed MD simulation of water (the ST2 model) near flat hydrophobic walls and proposed the picture of "dangling" hydrogen bonds; i.e., a water molecule prefers to take the orientation with one potentially hydrogen-bonding group toward the wall to balance the minimization of the energy and the maximization of the density. The similar result (the formation of an aligned ice structure) is obtained by Valleau *et al.*[61] for the TIPS2 water model[62] near inert walls. Linse[63] reported the MC simulation of the benzene–water interface and found the preferred alignment of water dipoles parallel to the surface and the reinforcement of the hydrogen bonding. We have not studied the character of the hydrogen-bonded network here, but the similar explanation would hold true for the liquid–vapor interface, contrary to the expectation[60] that the orientational preference would not be observed for these less regular surfaces.

VI. CONCLUSION

It was confirmed by molecular dynamics simulation that the thermodynamic properties of the liquid–vapor interface of water are much different from those of the Lennard-Jones system. In particular, the lowering of the surface excess entropy of water is the evidence of structural change near the surface, which can be related to the hydrophobic structural making. The orientational ordering was mainly investigated in this paper and two types were found: in the vapor side of the surface, a water molecule has its one H atom projecting toward the vapor phase and, in the liquid side, a molecule tends to lie down on the surface with its both H atoms slightly directed toward the liquid phase. These orientational orderings can be explained as the formation of ice structure, like the water near hydrophobic walls. As a result of such orientation, the surface potential χ, which is important, but controversial in electrochemistry, became positive. The ellipticity coefficient was estimated from the density profile with the Clausius–Mossotti formula, and the anisotropic effect of water due to the orientational ordering was found to be very small; the assumption that the density profile has a hyperbolic tangent form, however, is inadequate for water and may cause the experimentally observed "abnormality" of the water surface.

To study more detailed properties of water near the surface, such as two-body distribution functions and time-correlation functions, requires a much larger amount of computation that we cannot report here, but are planning to execute.

ACKNOWLEDGMENTS

We would like to thank Dr. Shuichi Nosé of Keio University for his kind advice about the MD simulation technique. We are also grateful to Professor Nobuhiro Gō of Kyoto University for valuable discussion. This work is supported in part by a grant in aid for Science Research (No. 61134043 and No. 62124039) from the Ministry of Education, Science, and Culture, and also by the Kyoto University Data Processing Center for using FACOM VP-200 and M-380, and the Computer Center of the Institute for Molecular Science for using HITAC S810/10 and M-680H.

[1] R. J. Good, J. Phys. Chem. **61**, 810 (1957).
[2] J. S. Rowlinson and B. Widom, *Molecular Theory of Capillarity* (Clarendon, Oxford, 1982).

[3]D. Beaglehole, in *Fluid Interfacial Phenomena*, edited by C. A. Croxton (Wiley, Chichester, 1986), Chap. 11.
[4]W. Drost-Hansen, Ind. Eng. Chem. **57-4**, 18 (1965).
[5]W. Drost-Hansen, J. Geophys. Res. **77**, 5132 (1972), and references therein.
[6]B. Borštnik, D. Janežič, and A. Ažman, Acta Phys. Acad. Sci. Hung. **48**, 297 (1980).
[7]O. Matsuoka, E. Clementi, and M. Yoshimine, J. Chem. Phys. **64**, 1351 (1976).
[8]C. Y. Lee and H. L. Scott, J. Chem. Phys. **73**, 4591 (1980).
[9]F. H. Stillinger and A. Rahman, J. Chem. Phys. **60**, 1545 (1974).
[10]R. M. Townsend, J. Gryko, and S. A. Rice, J. Chem. Phys. **82**, 4391 (1985).
[11]W. A. Weyl, J. Colloid Sci. **6**, 389 (1951).
[12]F. H. Stillinger and A. Ben-Naim, J. Chem. Phys. **47**, 4431 (1967).
[13]N. H. Fletcher, Philos. Mag. **18**, 1287 (1968).
[14]C. A. Croxton, Physica A **106**, 239 (1981).
[15]C. G. Gray and K. E. Gubbins, *Theory of Molecular Fluids* (Clarendon, Oxford, 1984), Vol. 1, Appendix D.
[16]W. H. Flygare and R. C. Benson, Mol. Phys. **20**, 225 (1971).
[17]N. K. Adam, *The Physics and Chemistry of Surfaces*, 3rd ed. (Oxford University, Oxford, 1941).
[18]E. A. Guggenheim, *Thermodynamics* (North–Holland, Amsterdam, 1949).
[19]S. Ono and S. Kondo, in *Encyclopedia of Physics*, edited by S. Flügge (Springer, Berlin, 1960), Vol. 10.
[20]F. P. Buff and R. A. Lovett, in *Simple Dense Fluids*, edited by H. L. Frisch and Z. W. Salsburg (Academic, New York, 1968).
[21]G. J. Gittens, J. Colloid Interface Sci. **30**, 406 (1969).
[22]R. Cini, G. Loglio, and A. Ficalbi, J. Colloid Interface Sci. **41**, 287 (1972).
[23]N. B. Vargaftik, B. N. Volkov, and L. D. Voljak, J. Phys. Chem. Ref. Data, **12**, 817 (1983).
[24]A. Braslau, M. Deutsch, P. S. Pershan, A. H. Weiss, J. Als-Nielsen, and J. Bohr, Phys. Rev. Lett. **54**, 114 (1985).
[25]K. Kinoshita and H. Yokota, J. Phys. Soc. Jpn. **20**, 1086 (1965), and references therein.
[26]M. C. Phillips, in *Water, A Comprehensive Treatise*, edited by F. Franks (Plenum, New York, 1975), Vol. 5, Chap. 3.
[27]J. Lekner, Mol. Phy. **49**, 1385 (1983).
[28]J. G. Kirkwood and F. P. Buff, J. Chem. Phys. **17**, 338 (1949).
[29]A. Harasima, Adv. Chem. Phys. **1**, 203 (1958). Another definition is in the paper of J. H. Irving and J. G. Kirkwood, J. Chem. Phys. **18**, 817 (1950).
[30]Y. Kataoka, J. Chem. Phys. **87**, 589 (1987).
[31]V. Carravetta and E. Clementi, J. Chem. Phys. **81**, 2646 (1984).
[32]W. Smith and D. Fincham, CCP5 newsletter (Daresbury Laboratory, Warrington, England, 1982).
[33]S. Nosé and M. L. Klein, Mol. Phys. **50**, 1055 (1983).
[34]J-P. Hansen and L. Verlet, Phys. Rev. **184**, 151 (1969).
[35]J. W. Cahn and J. E. Hilliard, J. Chem. Phys. **28**, 258 (1958).
[36]S. Fisk and B. Widom, J. Chem. Phys. **50**, 3219 (1969).
[37]F. P. Buff, R. A. Lovett, and F. H. Stillinger, Phys. Rev. Lett. **15**, 621 (1965).
[38]T. Nakagawa and Y. Oyanagi, in *Recent Developments in Statistical Inference and Data Analysis*, edited by K. Matusita (North–Holland, Amsterdam, 1980).
[39]R. C. Reid, J.M. Pravsnitz, and T. K. Sherwood, *The Properties of Gases and Liquids*, 3rd ed. (McGraw–Hill, New York, 1977), Appendix.
[40]W. A. P. Luck, Discuss. Faraday Soc. **43**, 115 (1967).
[41]A. N. Frumkin, Z. Phys. Chem. **109**, 34 (1924).
[42]B. Case and R. Parsons, Trans. Faraday Soc. **63**, 1224 (1967).
[43]A. N. Frumkin, Z. A. Iofa, and M. A. Gerovich, Zhur. Fiz. Khim. **30**, 1455 (1956).
[44]D. J. Schiffrin, Trans. Faraday Soc. **66**, 2464 (1970).
[45]F. Franks and D. S. Reid, in *Water, A Comprehensive Treatise*, edited by F. Franks (Plenum, New York, 1973), Vol. 2, Chap. 5.
[46]P. A. Egelstaff and B. Widom, J. Chem. Phys. **53**, 2667 (1970).
[47]I. C. Sanchez, J. Chem. Phys. **79**, 405 (1983).
[48]F. H. Ree, J. Chem. Phys. **73**, 5401 (1980).
[49]P. Drude, *The Theory of Optics* (Dover, New York, 1959).
[50]R. M. A. Azzam and N. M. Bashara, *Ellipsometry and Polarized Light* (North–Holland, Amsterdam, 1977).
[51]H. Fröhlich, *Theory of Dielectrics*, 2nd ed. (Clarendon, Oxford, 1958).
[52]W. F. Murphy, J. Chem. Phys. **67**, 5877 (1977).
[53]*Handbook of Chemistry and Physics*, 55th ed., edited by R. C. Weast (CRC, Cleveland, 1974).
[54]D. Beaglehole, Physica B **100**, 163 (1980).
[55]V. A. Kizel', J. Exp. Theor. Phys. USSR **29**, 658 (1955).
[56]S. M. Thompson, K. E. Gubbins, and J. M. Haile, J. Chem. Phys. **75**, 1325 (1981).
[57]J. Eggebrecht, K. E. Gubbins, and S. M. Thompson, J. Chem. Phys. **86**, 2286 (1987).
[58]E. Chacon, P. Tarazona, and G. Navascués, J. Chem. Phys. **79**, 4426 (1983).
[59]E. Chacon, L. Mederos, G. Navascués, and P. Tarazona, J. Chem. Phys. **82**, 3802 (1985).
[60]C. Y. Lee, J. A. McCammon, and P. J. Rossky, J. Chem. Phys. **80**, 4448 (1984).
[61]J. P. Valleau and A. A. Gardner, J. Chem. Phys. **86**, 4162 (1987).
[62]B. Jorgensen, J. Chem. Phys. **77**, 4156 (1982).
[63]P. Linse, J. Chem. Phys. **86**, 4177 (1987).

The Journal of Chemical Physics is copyrighted by the American Institute of Physics (AIP). Redistribution of journal material is subject to the AIP online journal license and/or AIP copyright. For more information, see http://ojps.aip.org/jcpo/jcpcr/jsp
Copyright of Journal of Chemical Physics is the property of American Institute of Physics and its content may not be copied or emailed to multiple sites or posted to a listserv without the copyright holder's express written permission. However, users may print, download, or email articles for individual use.

The Journal of Chemical Physics is copyrighted by the American Institute of Physics (AIP). Redistribution of journal material is subject to the AIP online journal license and/or AIP copyright. For more information, see http://ojps.aip.org/jcpo/jcpcr/jsp